Optical and Quantum Electronics (2023) 55:1212
https://doi.org/10.1007/s11082-023-05542-w

Characterization and linear/nonlinear optical properties of PVA/CS/TiO_2 polymer nanocomposite films for optoelectronics applications

M. R. El-Aassar[1] · Rabab K. Sendi[2] · A. Atta[3] · Nuha Al-Harbi[2] · Mohamed Rabia[4,5] · M. M. Abdelhamied[6]

Received: 25 April 2023 / Accepted: 4 October 2023 / Published online: 21 October 2023

Abstract
Polymer composite materials combines of polyvinyl alcohol (PVA), chitosan (CS), and titanium oxide (TiO_2) were successfully synthesizing for using in optoelectronics. Successful incorporation of TiO_2 into the PVA/Chitosan (PVA/CS) blend matrix has been demonstrated by XRD, AFM, FTIR and SEM. The TiO_2 is uniformly loaded and distributed in polymer chain, as seen by SEM and AFM images. Using UV–Vis optical spectroscopy, we determine the absorption coefficient, band edge, carbon clusters numbers, and Urbach energy. The effects of TiO_2 on linear/nonlinear optical characteristics were investigated. The band gap of PVA/CS/TiO_2 is reduced when compared to PVA/CS. However, the absorbance and optical conductivity were both increased by TiO_2. After mixed PVA/CS with 2.5%, 7.5%, and 10% TiO_2, the band gap energy drops from 4.99 for PVA/CS to 4.9, 4.7, and 4.23 eV, while the Urbach tail of the blend is 1.01 eV, it enhanced to 1.45 eV, 1.72 eV, and 2.07 eV respectively. The values of relaxation time τ decrease gradually from 2.35×10^{-5} s to 1.11×10^{-5}, 1.87×10^{-6} to 1.69×10^{-6} s as the concentration of TiO_2 is raised from 2.5 to 7.5% and 10%. It has been found that incorporating TiO_2 into PVA/CS enhances the synthetic composite's optical characteristics, making the composite PVA/CS/TiO_2 it suitable for use in both energy applications and optoelectronics.

Keywords Nanocomposite · Synthesis · Structural · Optical · Energy applications

1 Introduction

Flexible composite materials are expanding rapidly to develop with suitable qualities for portable and wearable electronics devices (Althubiti et al. 2023a, b). Researchers are paying special attention to the structures, mechanical qualities, and electronic properties of polymeric films (Atta et al. 2023). Because of their special properties like portability, shape versatility, adaptability, and low cost (Alotaibi et al. 2023a; Ahmad Fauzi et al. 2022), Many researchers are looking on conductive polymer composites for usage in electronics. The composite's exceptional properties make it suitable for use in lightweight and flexible electronics. This has led to a significant amount of focus

Extended author information available on the last page of the article

on developing methods for making flexible composite films that incorporate conductive nanoparticle materials (Mohamed et al. 2022; Iqubal 2022). Flexible nanocomposites are becoming a novel material for a variety of energy devices (Ashour et al. 2021). Because inorganic fillers stimulate internal processes like carbonization and macromolecular dispersion, they are able to alter the optical characteristics of the polymer composite upon addition to the polymer matrix (Mohanraj et al. 2018).

PVA/Chitosan (PVA/CS) blend has high features of chemical and mechanical characteristics (Alotaibi et al. 2023b), making it a versatile additive for a wide range of uses thanks to its high degree of transparency. PVA/CS is chosen as environmentally material with hydroxyl groups for sustainable and efficient methods for preparing composites. PVA/CS has unique characteristics such soluble, inexpensive, and consequently ecofriendly (Shubha and Madhusudana Rao 2016).

The properties of PVA is modified because the alignment of ions from the dissociated filler with the polar groups of PVA, resulting in the formation of a charge-transfer complex (Abdullah et al. 2015). So, by incorporating nanofillers into PVA, the PVA chemical properties is modified (Taghizadeh and Sabouri 2013). Researchers have tried to improve PVA physical properties by lowering the host polymer's crystalline phase by adding various nano-sized fillers to the PVA matrix (Arya et al. 2018). When crystallization is inhibited in a semi-crystalline host polymer, segmental chain mobility is enhanced (Saeed and Abdullah 2021; Hameed et al. 2021). In contrast, Chitosan is a biopolymer comprised of hydrophilic cationic linear polysaccharide. Chitosan has a distinct chemical makeup as a positively charged polyamine. Unique characteristics include film formation, gel formation, pH sensitivity, amenability to alteration and liquid absorption. These characteristics are making chitosan useful in systems and biosensors (Rosli et al. 2021).

The structural and optical properties of TiO_2 have made them a popular choice among inorganic fillers (Ullah et al. 2018). Because of their unique properties, as well as the numerous potential uses in industry, TiO_2 nanoparticles have attracted a lot of attention (Naseem et al. 2021). TiO_2 nanoparticles are widely used in different devices like sensors and solar cells. In addition, TiO_2 is a promising materials with novel characteristics for several applications such as super capacitors rechargeable batteries. The current study focuses on incorporation of conductive TiO_2 fillers into a PVA/CS matrix to improve optical efficiency. TiO_2 in polymers exhibits novel properties for usage in photonics and capacitors to store electrical charges (Begum et al. 2021).

The TiO_2 is a direct semiconductor bandgap with favorable optical properties that used in light-emitting diodes (LEDs) and solar cells (Aziz et al. 2018). TiO_2 filler is the most studied oxides has energy gap of 3.05 eV (Hadi et al. 2020), making it a direct bandgap semiconductor. In contrast, Abdullah et al. (2017) found that CO_2 conversion was significantly enhanced by TiO_2. When CO_2 is reduced via photo catalysis, the distribution of the resulting products is extremely sensitive to the band gap of the catalyst. Additionally, Aziz et al. (2019) used a solution cast approach to create a composite of chitosan/NH_4Tf/TiO_2 electrolytes. Up to 1 wt% of TiO_2 was found to increase the dielectric characteristics of composite electrolytes. Additionally, Abdullah et al. (2023) investigated TiO_2 modified the physical and electrical characteristics of PVA-NH_4NO_3. They found that the ionic conductivity is significantly improved after adding TiO_2NPs single-crystal.

The distinctive aspect of this research is the inclusion of TiO_2 into PVA/CS at varying concentrations for use in optoelectronics. FTIR, XRD, SEM, and AFM analyses all corroborate that PVA/CS/TiO_2 nanocomposites have formed successfully. Structure and linear/nonlinear optical characteristics of PVA/CS as a function of TiO_2 filler were investigated.

This work shows that flexible PVA/CS/TiO_2 were successfully prepared and their linear/nonlinear characteristics were improved for use in optoelectronics devices.

2 Materials and Methods

PVA, molecular weight of 84,500–89,500 g/mol, titanium dioxide (TiO_2) of particle size of 20 nm, chitosan with a degree of deacetylation 84% were provided from Sigma-Aldrich Co., USA. The polymer solutions were prepared separately for the preparation of cross-linked PVA/CS/TiO_2 blended membranes. 1 gm of PVA is dissolving in 100 ml of deionized water at 75 °C with stirring for 1.5 h, and 1 gm of chitosan was stirred into 95 ml of acetic acid solution at room temperature. The PVA and CS were combined and stirred for 7 h. In order glutaraldehyde was used as a cross-linked the composite after various concentrations of TiO_2 were added to the solution. The TiO_2NPs were then uniformly dispersed in the PVA/CS blend by sonicating the mixtures for 40 min. Drying time was achieved by pouring the completed PVA/CS/TiO_2 mixture onto a glass Petri dish, removing any remaining air bubbles with a combination of shaking and blowing. To achieve the desired results, this process was performed multiple times to obtain 2.5%, 7.5% and 10% of TiO_2 in PVA/CS. The mean thickness of the created sheets in the range of 0.1 mm is measured with a thickness gauge (Mitutoyo 7301).

XRD (XRD-6000) in 2θ of 4° to 80° and FTIR (ATI Mattson, England) in wavelength of 500 to 4000 cm^{-1} were used for investigating the structural characteristics of PVA/CS/TiO_2. The SEM images were captured using a FE-SEM (SEM, JEOL, Japan). The changes in surface morphology and roughness OF PVA/CS/TiO_2 are investigated with AFM. The optical spectra were given by the UV/VIS optical spectrophotometer (double-beam JascoV-670) in range of 200 to 1050 nm.

3 Results and Discussion

Figure 1 investigates the XRD of PVA/CS, 0.025TiO_2, 0.075TiO_2, and 0.1TiO_2. The pure PVA/CS spectrum shows diffraction peak at 20.1°, while the XRD of PVA/CS/TiO_2 show other new diffraction peaks at 25.4°. The XRD show a further reduction in the PVA/CS diffraction peak of 20.1° by increasing TiO_2. This decrease in PVA/CS crystallinity indicated the interaction between the PVA/CS chains and TiO_2. The changes of FWHM of PVA/CS peak at 20.1° have proved a good interaction of the PVA/CS and TiO_2. The crystallite size (D) of the pure TiO_2 is calcuated using the simple Debye–Scherrer (Atta et al. 2021).

$$D = \frac{0.94\lambda}{\beta\cos\theta} \tag{1}$$

λ is the wavelength, θ is the diffraction angle, and β is refer to FWHM. The crystallite size D, is determined of 35.2 nm

The FTIR spectra of synthesized PVA/CS, 0.025TiO_2, 0.075TiO_2, and 0.1TiO_2 are presented in Fig. 2. Broad peaks at 3290 cm^{-1} of PVA/CS could be attributed to –OH groups (Chhabra et al. 2020) and another at 2930 cm^{-1} for C–H stretching (Ismail et al. 2012). The other peaks at 1640 cm^{-1} attributed to vibrational C=C (Borhade and Uphade 2012). Beaks at ~ 1410 and 1080 cm^{-1} refers respectively to the –OH and C=O stretching. The band 908 cm^{-1} is assigned to C–C stretching and 825 cm^{-1} for CH_2 stretches. Due to the

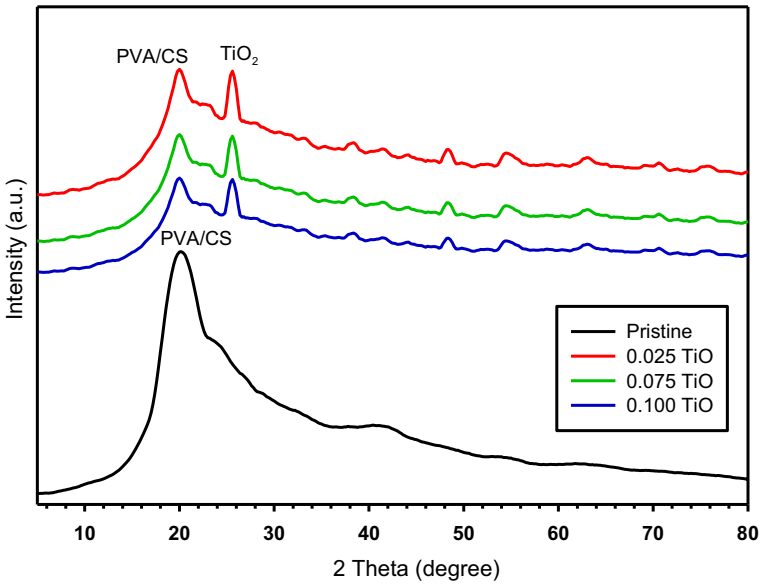

Fig. 1 XRD pattern of PVA/CS, $0.025TiO_2$, $0.075TiO_2$, and $0.1TiO_2$ films

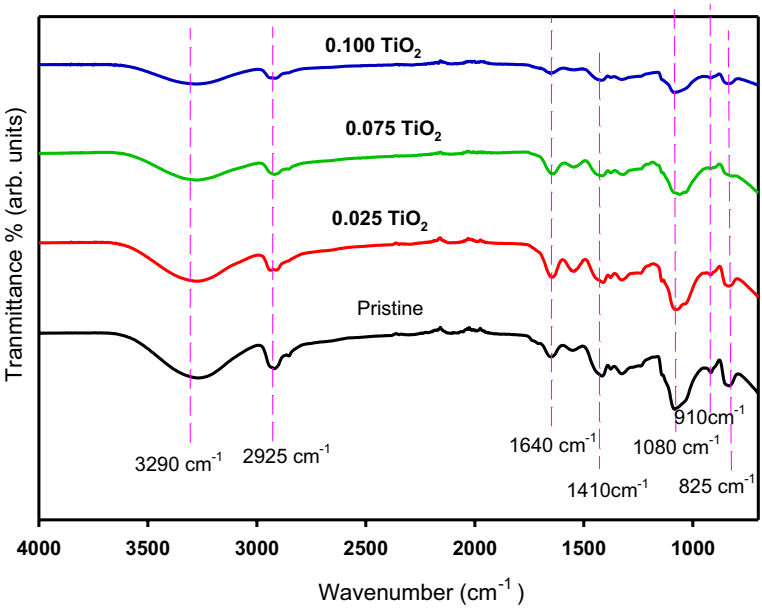

Fig. 2 FTIR of PVA/CS, $0.025TiO_2$, $0.075TiO_2$, and $0.1TiO_2$ films

interaction between TiO_2 and PVA/CS levels, a slight shift of the peaks were seen (Sayyah et al. 2015). Moreover, due to charge transport complexes, PVA/CS /TiO_2 composite films have a different intensity than pure PVA/CS (Khmissi et al. 2016). When nanoparticles

were added, these bands' locations were seen to shift from red to blue, clearly showing a change in the interactions between intermolecular hydrogen bonds and confirming the complexation between the polymer and the nanoparticles.

The SEM images show homogeneous morphology of PVA (Shi et al. 2015) with smooth surface and structure (Fig. 3a). Figure 3b–d are show SEM images of $0.025TiO_2$, $0.075TiO_2$, and $0.1TiO_2$ films, respectively. These images demonstrated the formation of nanocomposites with roughly shaped pores of varying sizes. The combination of PVA and TiO_2 is investigated the homogeneous surface morphologies. The bonding between the PVA chain and TiO_2 is due to this coalescence between polymer and TiO_2. Circular spots are uniformly distributed across the surface, forming fine discharge channels (Masid Roy et al. 2017). This suggests the formation of PVA/CS/TiO_2 nanocomposites. The scanning electron microscopy show TiO_2 nanoparticles are agglomerated uniformly in PVA/CS. Results from the FE-SEM analysis corroborate the XRD findings of a robust interaction between the polymer blend and TiO_2. Clearly, the PVA in these images has a thickness of around 90 um. TiO_2 nanoparticles fill the polymeric spaces in PVA, drawing the PVA chains closer together to form a dense hybrid structure.

Topographical views of PVA/CS and PVA/CS/TiO_2 in 2D were indicated in Fig. 4a, b, while 3D representations are shown in Fig. 4c, d, respectively. When compared with the PVA/TiO_2, which is characterized by nano convolutions, the topography of PVA is relatively smooth, according to AFM pictures. Addition of TiO_2 in PVA/CS is causes an increase in surface roughness, demonstrating that the mixed of TiO_2 in PVA/CA blend. Although PVA possesses hydrophilic channels, they have been constricted to provide a surface with a low roughness and high smoothness. Hydrophilic channels in PVA/CS blend

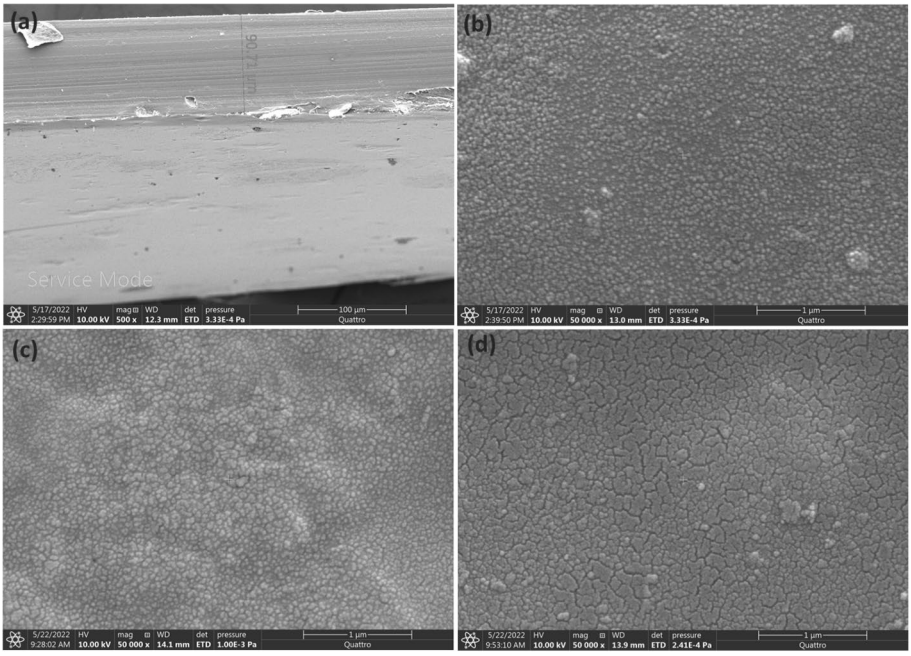

Fig. 3 SEM of **a** PVA/CS, **b** $0.025TiO_2$, **c** $0.075TiO_2$ and **d** $0.1TiO_2$ films

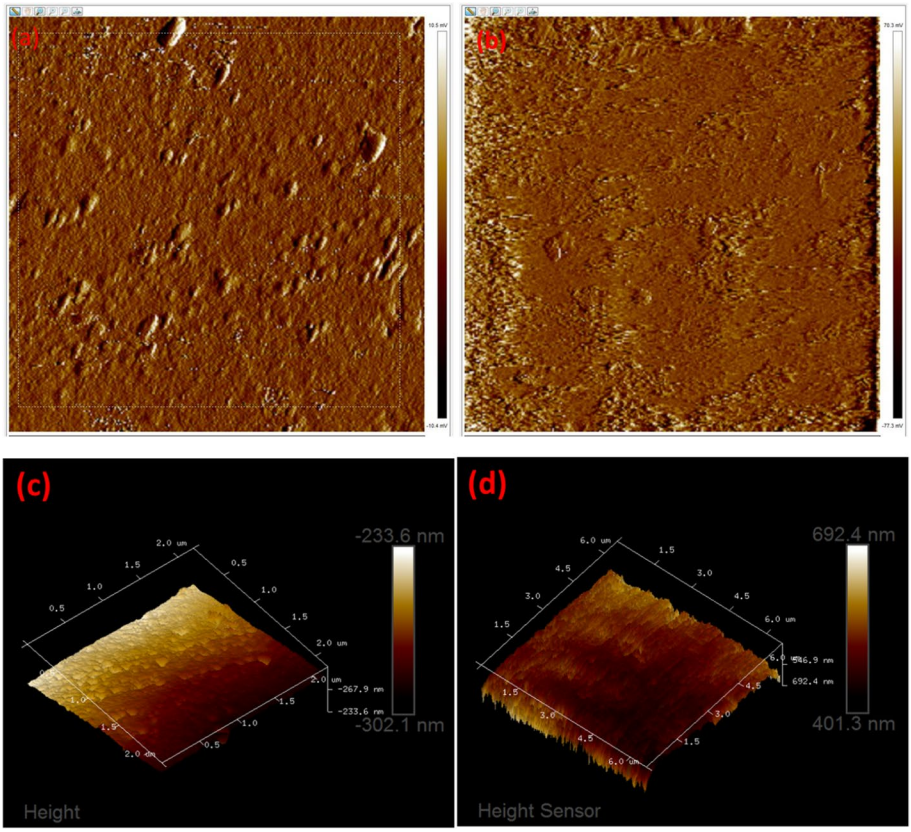

Fig. 4 2D AFM **a** PVA/CS, **b** 0.1TiO_2, 3D images of **c** PVA/CS and **d** 0.1TiO_2 films

are efficiently covered by the extra TiO_2 nanoparticles, making the PVA/CS/TiO_2 composite is rougher.

Figure 5a shows the absorbance of PVA/CS, 0.025TiO_2, 0.075TiO_2, and 0.1TiO_2 films. The band gap absorption of TiO_2 and absorption structural defects is both responsible for the uniform absorption behavior observed across all samples, which has an absorption peak around 650 nm. The TiO_2 content of the composite all have a significant impact on the absorption peak strength. As shown in Fig. 5a, the intensity are enhanced as the TiO_2 percentage was raised from 0.025 to 0.10. The findings are consistent with SEM findings and XRD data. The high peak with TiO_2 compared to PVA/CS is also demonstrated by the absence of a shift in the absorption peaks with increasing TiO_2. It is shown that the encapsulation of TiO_2 effects on the formation of TiO_2 and PVA/CS chains (Rao et al. 2012). The absorption coefficients (α) of PVA/CS/TiO_2 films is given by

$$\alpha = \frac{2.303A}{d} \tag{2}$$

A is absorbance and d is thickness. In Fig. 5b, the α is plotted with incident photon energy ($h\nu$). The α is rise as the TiO_2 content is increased. This change could be a result of the TiO_2 addition induced level changes (Taha et al. 2019). When 2.5%, 7.5%, and 10%

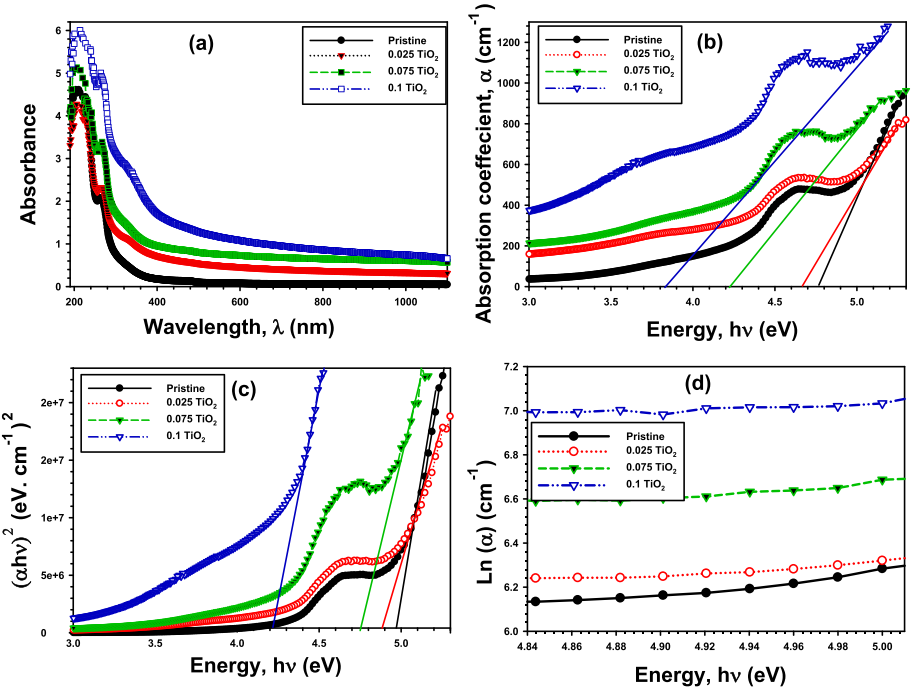

Fig. 5 **a** Absorbance with λ, **b** α versus $h\nu$, **c** band gap with $h\nu$ **d** ln (α) with $h\nu$

TiO_2 are added, the absorption edge of PVA/CS drops from 4.77 eV to 4.66, 4.21, and 3.81 eV, respectively. Tauc's relation is used to estimate the optical gap E_g by.

$$\alpha h\nu = A(h\nu - E_g)^m \tag{3}$$

Absorption constant is denoted by A, energy bandgap by E_g, and optical transition type by m. The relationship of $(\alpha\ h\nu)^2$ and photon energy (hν) is used to estimate the band gap E_g. This is achieved by extrapolating the straight line sections of the graphs to zero absorption, as in Fig. 5c and detailed in Table 1. The E_g is decreased as the TiO_2 increased. After being mixed with 2.5%, 7.5%, and 10% TiO_2, the E_g of the polymer drops from 4.99 to 4.9, 4.7, and 4.23 eV, respectively. Due to an enhancement of charge-carrier, the energy gap is varied by TiO_2. Taha et al. (2019), investigated the addition of nickel oxide (NiO) to PVC, and nearly the found the same behaviour. As NiONPs

Table 1 E_e, E_u and E_g values of PVA/CS, $0.25TiO_2$, $0.75TiO_2$, and $0.1TiO_2$

# Sample	E_e (eV)	E_g(eV)	E_u (eV)	Carbon number (N)
Pristine (PVA/CS)	4.77	4.99	1.01	166
$0.025TiO_2$	4.66	4.90	1.45	172
$0.075TiO_2$	4.21	4.70	1.72	178
$0.10TiO_2$	3.81	4.23	2.07	188

content increased and states were produced inside the optical band gap, they discovered the band gap shrank. This confirmed the miscibility of TiO_2 and PVA chains. Using relation $E_g = 34.4/N$, the optical gap E_g is used to estimate carbon cluster number (N) (Zaki et al. 2017). Table 1 displays the predicted N values for PVA/CS and PVA/CS/TiO_2. By increasing the TiO_2 content from 2.5 to 7.5% and 10%, the N value for PVA/CS rises from 166 to 172, 178 and 188. TiO_2 contributes to a lower band gap and higher N. The Urbach's tail is given according to formula (Zaki et al. 2017).

$$\alpha(\nu) = \alpha_o e^{h\nu/E_u} \tag{4}$$

where α_o is a constant and E_u is the band tail. As a result, the band tail of polymer and polymer/TiO_2 films is determined by plotting ln (α) with photon energy, as in Fig. 5d. The band tail of the polymer blend and composite samples was estimated using the inverse slope of the linear portions of these graphs, and the results are shown in Table 1. The predicted Urbach tail of the blend is 1.01 eV, it increases to 1.45 eV, 1.72 eV, and 2.07 eV by increasing TiO_2 to 2.5%, 7.5%, and 10% of TiO_2, respectively. Increases in the TiO_2 content of the composite are associated with an increase in Urbach tail values, which is indicative of changes in disorder state. Furthermore, the structural characteristics of the blend were altered by TiO_2, which enhanced the optical properties. Graphene oxide (fGO) embedded in PVC exhibits similar behavior, the Urbach energies increasing with increased graphene oxides as a result of disorder in the nanocomposite (Taha and Saleh 2018).

The extinction coefficient (K_0) is given by (Kakil et al. 2018)

$$K_o = \frac{\alpha\lambda}{4\pi} \tag{5}$$

The K_0 of PVA/CS/TiO_2 are plotted with photon energy in Fig. 6a. It is crucial to understand that the increase in defects leads to an enhancement in the absorbance coefficient, which in turn raises K_o for composite samples. The reflectance of the samples with wavelengths is shown in Fig. 6b. The reflectance of PVA/CS/TiO_2 changes with wavelength. The composite's reflectivity also changed as the TiO_2 content was increased. The refractive index (n) is given by (Alrowaili et al. 2021).

$$n = \frac{(1+R)}{(1-R)} + \sqrt{\frac{4R}{(1-R)^2} - K_o{}^2} \tag{6}$$

The index of pure PVA/CS and PVA/CS/TiO_2 nanocomposite samples is shown in Fig. 6c. The index n rises with wavelength in both pure and composite films. The refractive index gradually changed after pure PVA/CS was mixed with 2.5%, 7.5%, and 10% TiO_2. Covalent bonds can be formed between different chains thanks to the composite's increased TiO_2 (Obasi et al. 2019). The optical conductivity of PVA/CS and PVA/CS/TiO_2 given by Banerjee and Kumar (2011).

$$\sigma_{opt} = \frac{\alpha nc}{4\pi} \tag{7}$$

Figure 6d shows the optical conductivity with wavelength. Because of the density of the concentrated states in the band structure, the conductivity of the films rises. Similar effects are seen when SnO_2 is added to PVC polymers, where higher concentrations of SnO_2 result in higher optical conductivities (Taha et al. 2018).

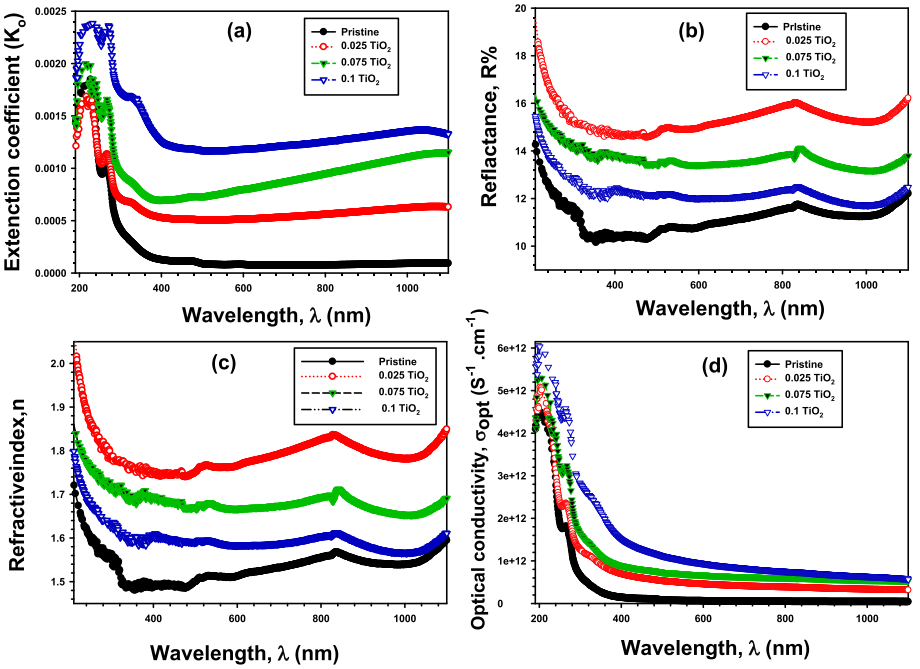

Fig. 6 Variation of **a** K_o with $h\nu$, **b** R with λ, **c** refractive index with λ, and **d** the optical conductivity with λ, for PVA/CS, $0.025TiO_2$, $0.075TiO_2$, and $0.1TiO_2$

Real ε_r and imaginary ε_i are the two terms that make up a material's complex dielectric constant, which is one of its most crucial characteristics (Donya et al. 2020).

$$\varepsilon = \varepsilon_r + i\varepsilon_i \tag{8}$$

The next formula is to estimate the ε_r (Abd El-Rahman et al. 2019).

$$\varepsilon_r = n^2 - {K_o}^2 \tag{9}$$

The real component (ε_r) is changes with wavelength as shown in Fig. 7a. As was already mentioned, adding TiO_2 to the PVA/CS results in the formation of covalent bonds between individual chains, leading to an enhanced in the loss of photon energy. The fictitious component, which represents the energy dissipation caused by the motion of the dipole moment, is also obtained from relation (Rasheed et al. 2019).

$$\varepsilon_i = 2nK_o \tag{10}$$

The ε_i versus wavelength of PVA/CS/TiO_2 is shown in Fig. 7b.

Thus, the dispersion of refractive index is alternatively investigated by using the single oscillator model (Wemple DiDomenicon model) by Equation (Abdullah et al. 2022).

$$\frac{1}{n^2-1} = \frac{E_O}{E_d} - \frac{1}{E_O E_d}(h\nu)^2 \tag{11}$$

E_o denotes the singular oscillating energy and E_d the dispersion energy.

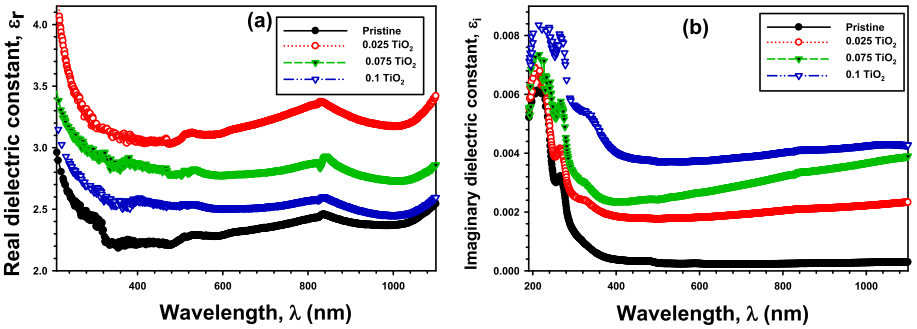

Fig. 7 **a** real and **b** imaginary constants with λ, for PVA/CS, 0.025TiO_2, 0.075TiO_2, and 0.1TiO_2

The relationship between $(n^2-1)^{-1}$ and $(h\nu)^2$ of the pure PVA/CS and PVA/CS/TiO_2 films is depicted in Fig. 8a. The intercept and slope of the linear fitting component are used to calculate E_0 and E_d. Additionally, PVA/CS and PVA/CS/TiO_2 refractive static index values were provided by Al-Zahrani et al. (2015).

$$n_o = \left(1 + \frac{E_d}{E_O}\right)^{1/2} \tag{12}$$

Hence, the (ε_∞) of the PVA/CS /TiO_2 were estimated by $\varepsilon_\infty = (n_o)^2$. Table 2 summarizes the E_o, E_d, and n_o, for both PVA/CS/TiO_2 films. Including TiO_2 into the polymer with

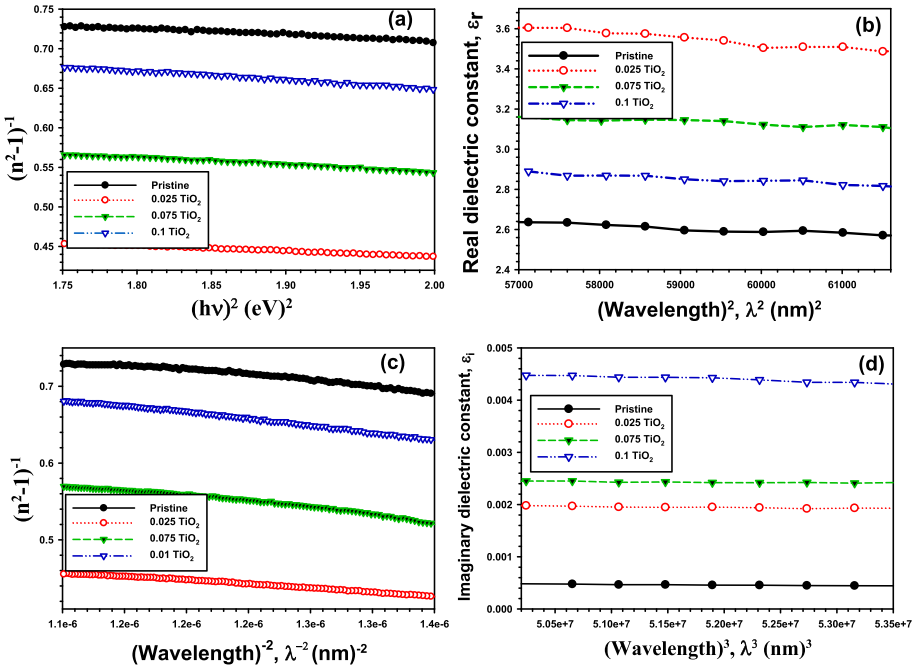

Fig. 8 **a** $(n^2-1)^{-1}$ against $(h\upsilon)^2$, **b** ε_r against λ^2, **c** $(n^2-1)^{-1}$ against λ^{-2}, and **d** ε_i against λ^3, PVA/CS, 0.025TiO_2, 0.075TiO_2, and 0.1TiO_2

Table 2 n_o, E_d, E_0, ε_∞, ε_l, and N/m^* for PVA/CS, $0.025TiO_2$, $0.075TiO_2$, and $0.1TiO_2$

# Sample	n_o	E_d (eV)	E_o (eV)	ε_∞	ε_l	$N/m^* \times 10^{41}$
Pristine (PVA/CS)	1.53	3.38	2.47	2.35	2.64	0.16
$0.025TiO_2$	1.51	3.56	2.42	2.51	2.87	0.19
$0.075TiO_2$	1.66	4.46	2.55	2.75	3.16	0.23
$0.1TiO_2$	1.81	5.89	2.65	3.29	3.61	0.31

2.5%, 7.5%, and 10%, is changed E_0 from 2.47 eV ($E_o = 0.495E_g$) for the pure PVA/CS to 2.42 eV ($E_o = 0.494E_g$), 2.55($E_o = 0.543E_g$) and 2.65 eV ($E_{oo} = 0.626E_g$). This indirect in relation between E_g and E_o is due to the aggregation of TiO_2 in the composite for high concentration of TiO_2. The dispersion energy E_d enhanced from 3.38 to 3.56, 4.46, 5.89 eV. In addition, as indicated in Table 2, the statically refractive index n_0 is 1.53 for PVA/CS and it changed to 1.51, 1.66, 1.81 when the TiO_2 concentration is increased from 2.5 to 7.5% and 10% respectively.

Dielectric constants are calculated using the Spitzer-Fan approach, which (N/m*) to identify the dielectric constant using (El-Nahass et al. 2009).

$$\varepsilon_r = \varepsilon_l - \left(\frac{e^2}{4\pi^2 \varepsilon_s c^2} \frac{N}{m^*} \right) \lambda^2 \tag{13}$$

The constant s is the dielectric free space constant, c is the speed of light, and e is the charge of an electron. Hence, Fig. 8b depicts the λ^2 and ε_r for the PVA/CS and PVA/CS/TiO_2. Table 3 displays the slope and interception of the straight sections of the detour, derived from the PVA/CS and PVA/CS/TiO_2 composites, respectively. The resonant plasma frequency (W_p) is determined by (Hamad 2013).

$$W_p = \frac{e^2}{\varepsilon_o} \times \frac{N}{m^*} \tag{14}$$

The addition of 2.5%, 7.5%, and 10% TiO_2 in PVA/CS led to an increase in N/m*, and Wp values. Additionally, medium oscillator (λ_o), the long refractive index (n_∞), and oscillator length intensity (S_o) are determined using the single-term Sellmeier oscillator method (Alwan 2012).

$$(n_\infty^2 - 1)/(n^2 - 1) = 1 - \left(\frac{\lambda_o}{\lambda} \right)^2 \tag{15}$$

Hence, the relationship of $(n^2-1)^{-1}$ and λ^{-2} at longer-wavelength is shown in Fig. 8c. As stated in Table 3, it is possible to estimate n_∞ and λ_0 from the intercept and slope of the linear portion of the detour, respectively. Thus, we can approximate S_0 values as (El Sayed et al. 2014).

$$S_o = (n_\infty^2 - 1)/(\lambda_o)^2 \tag{16}$$

The values of n_∞ increase, but the value of S_0 decreases, as the TiO_2 load increases. In the Drude model, ε_i is calculated using the following formula (Saadeddin et al. 2007).

Table 3 W_p, λ_o, S_o, n_∞, and τ of PVA/CS, $0.025TiO_2$, $0.075TiO_2$, and $0.1TiO_2$

# Sample	W_p ($\times 10^{15}$ s^{-1})	λ_o (nm)	S_o ($\times 10^5$ nm^2)	n_∞	τ ($\times 10^{-5}$ s)
Pristine(PVA/CS)	0.042	422.01	2.44	1.54	2.35
$0.025TiO_2$	0.051	494.97	1.66	1.57	1.11
$0.075TiO_2$	0.038	540.06	1.65	1.66	0.187
$0.1TiO_2$	0.089	446.98	0.91	1.80	0.169

$$\varepsilon_i = \frac{1}{4\pi^3 \varepsilon_o}\left(\frac{e^2 N}{c^3 m^* \tau}\right)\lambda^3 \tag{17}$$

The values for, the relaxation time, are thus calculated by plotting the relationship between ε_i and λ^3, as shown in Fig. 8d, and are tabulated below. The values of τ decrease gradually from 2.35×10^{-5} s to 1.11×10^{-5}, 1.87×10^{-6} to 1.69×10^{-6} s as the concentration of TiO_2 is raised from 2.5 to 7.5% and 10%. Based on these findings, it is clear that incorporating TiO_2 filler into PVA/CS results in nanocomposite films with enhanced properties, making TiO_2/PVA/CS films a practical choice for use in energy devices. Nonlinear optical (NLO) responsiveness of a material pattern is described by the following formula (Frumar et al. 2003):

$$P = X^{(1)}E + X^{(2)}E^2 + X^{(3)}E^3 \tag{18}$$

P represents the polarization, $X^{(1)}$ represents the first linear susceptibility, $X^{(2)}$ represents the second NLO susceptibility, and $X^{(3)}$ is the third NLO. Both $X^{(1)}$ and $X^{(3)}$ are calculated using (Ticha and Tichy 2002).

$$X^{(1)} = \frac{(n^2-1)}{4\pi} \tag{19}$$

and

$$X^{(3)} = A\left(X^{(1)}\right)^4 \tag{20}$$

The refractive index given by:

$$n(\lambda) = n_o(\lambda) + n_2\left(E^2\right) \tag{21}$$

The n_2 is estimated by (Kanis et al. 1991).

$$n_2 = \frac{12\pi X^{(3)}}{n_o} \tag{22}$$

Figure 9a, b demonstrate the relationship between $X^{(1)}$ and $X^{(3)}$ and for pure PVA/CS and PVA/CS/TiO_2 composites samples, respectively. As the percentage of TiO_2 in the composite increased, so did the amounts of $X^{(1)}$ and $X^{(3)}$. The introduction of TiO_2 causes an increase in local polarizabilities, which originates from the defects' centers (Ali et al. 2021). Non-linear refractive index versus wavelength for PVA/CS and PVA/CS /TiO_2 samples is also depicted in Fig. 9c. Notably, n_2 quantities grow in a linear fashion with increasing TiO_2 content in the composite, mirroring the behavior observed for Atta et al. (2023). Based on these results, it is clear that the PVA/CS /TiO_2 nanocomposite film is preferable to pure PVA/CS when it comes to nonlinear optical applications and optoelectronic devices.

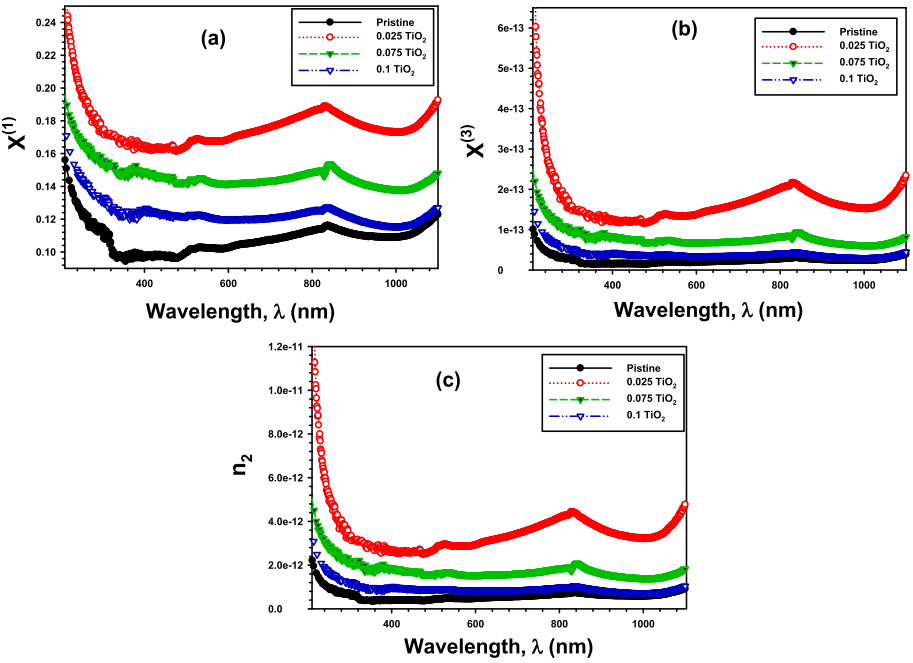

Fig. 9 **a** $X^{(1)}$, **b** $X^{(3)}$, and **c** n_2 versus the wavelength λ for PVA/CS, 0.025TiO_2, 0.075TiO_2, and 0.1TiO_2

4 Conclusion

The XRD, SEM, AFM and FTIR results verify the successful fabrication of PVA/CS/TiO_2 nanocomposites samples. The SEM images showed that the TiO_2 had been successfully integrated onto the PVA, with average particle sizes ranging in 90 nm. The FTIR analysis further revealed that the TiO_2 nanoparticles were dispersed throughout the PVA/CS matrix. Surface morphological changes in TiO_2/PVA/CS have been attributed to the introduction of defects and chain session process. The optical characteristics are also evaluated for both PVA/CS and PVA/CS/TiO_2. The addition of 2.5%, 7.5%, and 10% TiO_2 to pure PVA/CS reduced the band gap energy from 4.99 to 4.9 eV, 4.7 eV, and 4.23 eV, respectively. Moreover, the oscillating energy E_0 changed from 2.47 for the pure PVA/CS to 2.42 eV, 2.55 and 2.65 eV and the dispersion energy E_d increased from 3.38 to 3.56, 4.46, 5.89 eV The linear/nonlinear optical parameters of the influence of TiO_2 were determined. Based on these results, PVA/CS /TiO_2 films with different concentrations of TiO_2 nanoparticles are superior characteristics compared to PVA/CS to be used in energy-related applications.

Author contributions AA and MM wrote the main results, EA and MR reviewed the manuscript, NAH and RS shared the funding. All authors read and approved the final manuscript.

Funding The authors would like to thank the Deanship of Scientific Research at Umm Al-Qura University for supporting this work by Grant Code: (22UQU4340173DSR01).

Availability of data and materials The datasets generated during and/or analyzed during the current study are available from the corresponding author on reasonable request.

Declarations

Conflict of interest The authors declare no conflict of interest.

Ethical approval Not applicable (The Research is not involving the studies on human or their data.)

References

Abd El-Rahman, M., Yassien, K.M., Yassene, A.A.: Effect of gamma irradiation on the optical properties of epoxy resin thin films. Optik **183**, 962–970 (2019)

Abdullah, O.G., Tahir, D.A., Kadir, K.: Optical and structural investigation of synthesized PVA/PbS nanocomposites. J. Mater. Sci. Mater. Electron. **26**, 6939–6944 (2015)

Abdullah, H., Khan, M.M.R., Ong, H.R., Yaakob, Z.: Modified TiO_2 photocatalyst for CO_2 photocatalytic reduction: an overview. J. CO2 Util. **22**, 15–32 (2017)

Abdullah, O.G., Mustafa, B.S., Bdewi, S.F., Ahmed, H.T., Mohamad, A.H., Suhail, M.H.: Improved of the structural and Electrical properties of the proton-conducting PVA-NH_4NO_3 solid polymer electrolyte system by incorporating nanosized anatase TiO_2 single-crystal. J. Electron. Mater. **52**(6), 3921–3930 (2023)

Abdullah, O.G., Salh, D.M., Mohamad, A.H., Jamal, G.M., Ahmed, H.T., Mustafa, B.S., Suhail, M.H.: Linear and nonlinear optical characterization of dye–polymer composite films based on methylcellulose incorporated with varying content of methylene blue. J. Electron. Mater. 1–9 (2022)

Ahmad Fauzi, A.A., Osman, A.F., Alrashdi, A.A., Mustafa, Z., Abdul Halim, K.A.: On the use of dolomite as a mineral filler and co-filler in the field of polymer composites: a review. Polymers **14**(14), 2843–2876 (2022)

Ali, H.E., Abd-Rabboh, H.S., Awwad, N.S., Algarni, H., Sayed, M.A., et al.: Photoluminescence, optical limiting, and linear/nonlinear optical parameters of PVP/PVAL blend embedded with silver nitrate. Optik **247**, 167863–167877 (2021)

Alotaibi, B.M., Atta, A., Atta, M.R., Abdeltwab, E., Abdel-Hamid, M.M.: Modifying the optical properties of hydrogen-beam-irradiated flexible PVA polymeric films. Surf. Innov. **40**, 1–12 (2023)

Alotaibi, B.M., Atta, M.R., Abdeltwab, E., Atta, A., Abdel-Hamid, M.M.: Surface modifications and optical studies of irradiated flexible PDMS materials. Surf. Innov. **40**, 1–11 (2023)

Alrowaili, Z.A., Taha, T.A., El-Nasser, K.S., Donya, H.: Significant enhanced optical parameters of PVA-Y_2O_3 polymer nanocomposite films. J. Inorg. Organomet. Polym Mater. **31**(7), 3101–3110 (2021)

Althubiti, N.A., Al-Harbi, N., Sendi, R.K., Atta, A., Henaish, A.M.: Surface characterization and electrical properties of low energy irradiated PANI/PbS polymeric nanocomposite materials. Inorganics **11**(2), 74–91 (2023a)

Althubiti, N.A., Atta, A., Al-Harbi, N., Sendi, R.K., Abdelhamied, M.M.: Structural, characterization and linear/nonlinear optical properties of oxygen beam irradiated PEO/NiO composite films. Opt. Quant. Electron. **55**(4), 348–365 (2023b)

Alwan, T.J.: Gamma irradiation effect on the optical properties and refractive index dispersion of dye doped polystyrene films. Turk. J. Phys. **36**(3), 377–384 (2012)

Al-Zahrani, J.H., El-Hagary, M., El-Taher, A.: Gamma irradiation induced effects on optical properties and single oscillator parameters of Fe-doped CdS diluted magnetic semiconductors thin films. Mater. Sci. Semicond. Process. **39**, 74–78 (2015)

Arya, A., Sadiq, M., Sharma, A.L.: Effect of variation of different nanofillers on structural, electrical, dielectric, and transport properties of blend polymer nanocomposites. Ionics **24**, 2295–2319 (2018)

Ashour, G., Hussein, M., Sobahi, T.: Nanocomposite containing polyamide and GNS for enhanced properties. Synthesis and characterization. J. Umm Al-Qura Univ. Appl. Sci. **7**(1), 1–6 (2021)

Atta, A., Abdelhamied, M.M., Abdelreheem, A.M., Berber, M.R.: Flexible methyl cellulose/polyaniline/silver composite films with enhanced linear and nonlinear optical properties. Polymers **13**, 1225 (2021)

Atta, A., Negm, H., Abdeltwab, E., Rabia, M., Abdelhamied, M.M.: Facile fabrication of polypyrrole/NiO_x core–shell nanocomposites for hydrogen production from wastewater. Polym. Adv. Technol. (2023)

Aziz, S.B., Karim, W.O., Qadir, K.W., Zafar, Q.: Proton ion conducting solid polymer electrolytes based on chitosan incorporated with various amounts of barium titanate ($BaTiO_3$). Int. J. Electrochem. Sci. **13**, 6112–6125 (2018)

Aziz, S.B., Abdullah, O.G., Al-Zangana, S.: Solid polymer electrolytes based on chitosan: NH4Tf modified by various amounts of TiO_2 filler and its electrical and dielectric characteristics. Int. J. Electrochem. Sci. **14**(2), 1909–1925 (2019)

Banerjee, S., Kumar, A.: Swift heavy ion irradiation induced modifications in the optical band gap and Urbach's tail in polyaniline nanofibers. Nucl. Instrum. Methods Phys. Res. Sect. B **269**(23), 2798–2806 (2011)

Begum, R., Ahmad, G., Najeeb, J., Wu, W., Irfan, A., Azam, M., Nisar, J., Farooqi, Z.H.: Stabilization of silver nanoparticles in crosslinked polymer colloids through chelation for catalytic degradation of p-nitroaniline in aqueous medium. Chem. Phys. Lett. **763**, 138263 (2021)

Borhade, A.V., Uphade, B.K.: A comparative study on characterization and photocatalytic activities of TiO_2 and Co doped TiO_2 nanoparticles. Chalcogen. Lett. **9**(7), 299–306 (2012)

Chhabra, V.A., Kaur, R., Walia, M.S., Kim, K.H., Deep, A.: PVA/CHITOSAN/TiO_2 QD nanocomposite structure for visible light driven photocatalytic degradation of rhodamine 6G. Environ. Res. **186**, 109615 (2020)

Donya, H., Taha, T.A., Alruwaili, A., Tomsah, I.B.I., Ibrahim, M.: Micro-structure and optical spectroscopy of PVA/iron oxide polymer nanocomposites. J. Market. Res. **9**(4), 9189–9194 (2020)

El Sayed, A.M., El-Sayed, S., Morsi, W.M., Mahrous, S., Hassen, A.: Synthesis, characterization, optical, and dielectric properties of polyvinyl chloride/cadmium oxide nanocomposite films. Polym. Compos. **35**(9), 1842–1851 (2014)

El-Nahass, M.M., Farag, A.A.M., Abd-El-Salam, F.: Effect of gamma irradiation on the optical properties of nano-crystalline InP thin films. Appl. Surf. Sci. **255**(23), 9439–9443 (2009)

Frumar, M., Jedelský, J., Frumarova, B., Wagner, T., Hrdlička, M.: Optically and thermally induced changes of structure, linear and non-linear optical properties of chalcogenides thin films. J. Non-Cryst. Solids **326**, 399–404 (2003)

Hadi, J.M., Aziz, S.B., Mustafa, M.S., Brza, M.A., Hamsan, M.H., Kadir, M.F.Z., Ghareeb, H.O., Hussein, S.A.: Electrochemical impedance study of proton conducting polymer electrolytes based on PVC doped with thiocyanate and plasticized with glycerol. Int. J. Electrochem. Sci. **15**(5), 4671–4683 (2020)

Hamad, T.K.: Refractive index dispersion and analysis of the optical parameters of (PMMA/PVA) Thin film. Al-Nahrain Journal of Science **16**(3), 164–170 (2013)

Hameed, F.J., Ibrahim, I.M., Abdullah, O.G., Suhail, M.H.: Enhancing optical and electrical gas sensing properties of polypyrrole nanoplate by dispersing nano-sized tungsten oxide. ECS J. Solid State Sci. Technol. **10**(10), 107001 (2021)

Iqubal, S.M.: Characterization, surface morphology and microstructure of water soluble colloidal MnO_2 nanoflakes. J. Umm Al-Qura Univ. Appl. Sci. **8**(1–2), 33–36 (2022)

Ismail, N.S.M., Ramli, N., Hani, N.M., Meon, Z.: Extraction and characterization of pectin from dragon fruit (*Hylocereus polyrhizus*) using various extraction conditions. Sains Malaysiana **41**(1), 41–45 (2012)

Kakil, S.A., Sabr, B.N., Hana, L.S., Abbas, T.A.H., Hussin, S.Y.: Effects of a low dose of gamma radiation on the morphology, and the optical and the electrical properties of an ITO thin film as an electrode for solar cell applications. J. Korean Phys. Soc. **72**(5), 561–569 (2018)

Kanis, D.R., Ratner, M.A., Marks, T.J., Zerner, M.C.: Nonlinear optical characteristics of novel inorganic chromophores using the Zindo formalism. Chem. Mater. **3**(1), 19–22 (1991)

Khmissi, H., El Sayed, A.M., Shaban, M.: Structural, morphological, optical properties and wettability of spin-coated copper oxide; influences of film thickness, Ni, and (La, Ni) co-doping. J. Mater. Sci. **51**(12), 5924–5938 (2016)

Masid Roy, S., Rao, N.N., Herissan, A., Colbeau-Justin, C.: Polyaniline film-based wireless photo reactor for hydrogen generation through exciton mediated proton reduction. Polymer **112**, 351–358 (2017)

Mohamed, A.M., Alamri, H.R., Hamad, M.A.: Investigation on giant electrocaloric properties in ferroelectric polymer P (VDF-TrFE)(65/35). Russian J. Phys. Chem. A **96**(10), 2259–2264 (2022)

Mohanraj, K., Balasubramanian, D., Chandrasekaran, J., Bose, A.C.: Synthesis and characterizations of Ag-doped CdO nanoparticles for PN junction diode application. Mater. Sci. Semicond. Process. **79**, 74–91 (2018)

Naseem, K., Begum, R., Wu, W., Irfan, A., Nisar, J., Azam, M., Farooqi, Z.: Core/shell composite microparticles for catalytic reduction of p-nitrophenol: kinetic and thermodynamic study. Int. J. Environ. Sci. Technol. **18**, 1809–1820 (2021)

Obasi, C.O., Ahmad, A.S., Ikhioya, I.L., Ramalan, A.M.: Effect of gamma radiation (60Co) on the optical transmittance, energy band gap and absorption coefficient of ZnSe thin films. Int. J. Eng. Appl. Sci. Technol. **4**(8), 224–228 (2019)

Rao, C.V.S., Ravi, M., Raja, V., Bhargav, P.B., Sharma, A.K., Rao, V.N.: Preparation and characterization of PVP-based polymer electrolytes for solid-state battery applications. Iran. Polym. J. **21**(8), 531–536 (2012)

Rasheed, H.S., Abbas, I.A., Kadhum, A.J., Maged, H.C.: The effect of gamma irradiation on the optical properties of (PVA-PAA-Al_2O_3) films. AIP Conf. Proc. **2190**, 020013 (2019)

Rosli, N.A.H., Loh, K.S., Wong, W.Y., Lee, T.K., Ahmad, A.: Hybrid composite membrane of phosphorylated chitosan/poly (vinyl alcohol)/silica as a proton exchange membrane. Membranes **11**(9), 675 (2021)

Saadeddin, I., Pecquenard, B., Manaud, J.P., Decourt, R., Labrugère, C., Buffeteau, T., Campet, G.: Synthesis and characterization of single-and co-doped SnO_2 thin films for optoelectronic applications. Appl. Surf. Sci. **253**(12), 5240–5249 (2007)
Saeed, M.A., Abdullah, O.G.: Effect of structural features on ionic conductivity and dielectric response of PVA proton conductor-based solid polymer electrolytes. J. Electron. Mater. **50**, 432–442 (2021)
Sayyah, S.M., Shaban, M., Rabia, M.: m-Toluidine polymer film coated platinum electrode as a pH sensor by potentiometric methods. Sens. Lett. **13**(11), 961–966 (2015)
Shi, X.F., Xia, X.Y., Cui, G.W., Deng, N., Zhao, Y.Q., Zhuo, L.H., Tang, B.: Multiple exciton generation application of TiO_2 quantum dots in ZnO/ TiO_2/graphene oxide for enhanced photocatalytic activity. Appl. Catal. B **163**, 123–128 (2015)
Shubha, L., Madhusudana Rao, P.: Temperature characterization of dielectric permittivity and AC conductivity of nano copper oxide-doped polyaniline composite. J. Adv. Dielectr. **6**, 1650018 (2016)
Taghizadeh, M.T., Sabouri, N.: Biodegradation behaviors and water adsorption of poly (vinyl alcohol)/starch/carboxymethyl cellulose/clay nanocomposites. Int. Nano Lett. **3**, 1–8 (2013)
Taha, T., Saleh, A.: Dynamic mechanical and optical characterization of PVC/fGO polymer nanocomposites. Appl. Phys. A **124**, 600 (2018)
Taha, T., Ismail, Z., Elhawary, M.: Structural, optical and thermal characterization of PVC/SnO_2 nanocomposites. Appl. Phys. A **124**, 307 (2018)
Taha, T., Hendawy, N., El-Rabaie, S., Esmat, A., El-Mansy, M.: Effect of NiO NPs doping on the structure and optical properties of PVC polymer films. Polym. Bull. **76**, 4769–4784 (2019)
Ticha, H., Tichy, L.: Semiempirical relation between non-linear susceptibility (refractive index), linear refractive index and optical gap and its application to amorphous chalcogenides. J. Optoelectron. Adv. Mater. **4**(2), 381–386 (2002)
Ullah, R., Bilal, S., Shah, A.U.H.A., Rahman, G., Ali, K.: Ternary composites of polyaniline with polyvinyl alcohol and Cu by inverse emulsion polymerization: a comparative study. Adv. Polym. Technol. **37**, 3448–3459 (2018)
Zaki, M.F., Ali, A.M., Amin, R.M.: Effect of gamma irradiation on optical and chemical properties of cellulose nitrate thin films. J. Adhes. Sci. Technol. **31**(12), 1314–1327 (2017)

Authors and Affiliations

M. R. El-Aassar[1] · Rabab K. Sendi[2] · A. Atta[3] · Nuha Al-Harbi[2] · Mohamed Rabia[4,5] · M. M. Abdelhamied[6]

✉ A. Atta
aamahmad@ju.edu.sa

M. R. El-Aassar
mrelaassar@ju.edu.sa

Rabab K. Sendi
rksendi@uqu.edu.sa

Nuha Al-Harbi
nfhariby@uqu.edu.sa

Mohamed Rabia
mohamedchem@science.bsu.edu.eg

M. M. Abdelhamied
m_elbana52@yahoo.com

[1] Chemistry Department, College of Science, Jouf University, P.O. Box: 2014, Sakaka, Saudi Arabia

[2] Department of Physics, Faculty of Applied Sciences, Umm Al-Qura University, Mecca, Saudi Arabia

[3] Physics Department, College of Science, Jouf University, P.O. Box: 2014, Sakaka, Saudi Arabia

[4] Nanomaterials Science Research Laboratory, Chemistry Department, Faculty of Science, Beni-Suef University, Beni-Suef 62514, Egypt

[5] Nanophotonics and Applications Lab., Physics Department, Faculty of Science, Beni-Suef University, Beni-Suef 62514, Egypt

[6] Charged Particles Lab., Radiation Physics Department, National Center for Radiation Research and Technology (NCRRT), Egyptian Atomic Energy Authority (EAEA), Cairo, Egypt